JPET Fast Forward. Published on August 28, 2017 as DOI: 10.1124/jpet.117.243477
This article has not been copyedited and formatted. The final version may differ from this version.

Manuscript title: Heterogeneous binding and CNS distribution of the multi-targeted kinase inhibitor ponatinib restrict orthotopic efficacy in a patient-derived xenograft model of glioblastoma

Authors: Janice K. Laramy, Minjee Kim, Shiv K. Gupta, Karen E. Parrish, Shuangling Zhang, Katrina K. Bakken, Brett L. Carlson, Ann C. Mladek, Daniel J. Ma, Jann N. Sarkaria, and William F. Elmquist

Brain Barriers Research Center, Department of Pharmaceutics, College of Pharmacy, University of Minnesota, Minneapolis, Minnesota (J.K.L, M.K, K.E.P., S.Z., W.F.E.); Department of Radiation Oncology, Mayo Clinic, Rochester, Minnesota (S.K.G, K.K.B, B.L.C, A.C.M, D.J.M, J.N.S)

Running title: Binding and delivery limit ponatinib efficacy in GBM

Corresponding author

William F. Elmquist

Professor

Department of Pharmaceutics

University of Minnesota

308 Harvard ST SE

Minneapolis MN 55455

Phone: 612-625-0097; fax: 612-626-2125

e-mail: elmqu011@umn.edu

Number of pages

Number of text pages: 18

Number of tables: 2

Number of figures: 8

Number of references: 39

Number of words in abstract: 228

Number of words in introduction: 742 words (excluding in-text citations)

Number of words in discussion: 1,483 words (excluding in-text citations)

Supplemental table: 1

Supplemental figure: 1

Abbreviations

AUC, area under the curve

BAT, brain-around-tumor

BBB, blood-brain barrier

BEV, bevacizumab

CL/F, apparent clearance

Cmax, maximum drug concentration

CNS, central nervous system

JPET Fast Forward. Published on August 28, 2017 as DOI: 10.1124/jpet.117.243477
This article has not been copyedited and formatted. The final version may differ from this version.

DA, distribution advantage

ERL, erlotinib

fu, free (unbound) fraction

FVB, Friend leukemia virus strain B

GBM, glioblastoma

GFP, green fluorescent protein

IC, intracranial

IC_{50}, the half maximal inhibitory concentration

Kp, brain-to-plasma ratio

Kp,uu, unbound (free) brain-to-plasma ratio

LC-MS/MS, liquid chromatography–tandem mass spectrometry

NCA, noncompartmental analysis

PBS, phosphate buffered saline

PDGFR-alpha, platelet-derived growth factor receptor-alpha

PDX, patient-derived xenograft

RED, rapid equilibrium dialysis

RET, REarranged during Transfection

TMZ, temozolomide

Tmax, time at the maximum drug concentration

Vd/F, apparent volume of distribution

Recommended section assignment: Drug Discovery and Translational Medicine

JPET Fast Forward. Published on August 28, 2017 as DOI: 10.1124/jpet.117.243477
This article has not been copyedited and formatted. The final version may differ from this version.

ABSTRACT

This study investigated how differences in drug distribution and free fraction at different tumor and tissue sites influence the efficacy of the multi-kinase inhibitor ponatinib in a patient-derived xenograft (PDX) model of glioblastoma (GBM). Efficacy studies in GBM6 flank (heterotopic) and intracranial (orthotopic) models showed that ponatinib is effective in the flank but not in the intracranial model, in spite of a relatively high brain-to-plasma ratio. In vitro binding studies indicated that flank tumor had a higher free (unbound) drug fraction than normal brain. The total and free drug concentrations, along with the tissue-to-plasma ratio (Kp) and its unbound derivative (Kp,uu), were consistently higher in the flank tumor than the normal brain at 1 and 6 hours after a single dose in GBM6 flank xenografts. In the orthotopic xenografts, the intracranial tumor core displayed higher Kp and Kp,uu values compared to the brain-around-tumor (BAT). The free fractions and the total drug concentrations, hence, free drug concentrations, were consistently higher in the core than in the BAT at 1 and 6 hours post dose. The delivery disadvantages in the brain and BAT were further evidenced by the low total drug concentrations in these areas that did not consistently exceed the in vitro cytotoxic concentration (IC_{50}). Taken together, the regional differences in free drug exposure across the intracranial tumor may be responsible for compromising efficacy of ponatinib in orthotopic GBM6.

INTRODUCTION

Glioblastoma (GBM) is the most common malignant brain tumor in adults, and it is estimated that there will be about 12,000 new cases of GBM in 2017 (Ostrom et al., 2016). To date, no therapeutic agents other than temozolomide (TMZ) and bevacizumab (BEV) have improved the overall survival (TMZ) or symptoms (BEV) in GBM clinical trials in the past decade (Minniti et al., 2009). Despite of rigorous therapies that typically combine surgery, radiation, and chemotherapy, only about 17% of patients with GBM survive 2 years or longer (Ostrom et al., 2016). A large number of potent small molecule compounds have failed to demonstrate efficacy in GBM clinical trials. Although reasons for this lack of progress are multifactorial, the majority of small molecule compounds have limited distribution to the brain (Oberoi et al., 2016). Many GBMs have partial disruption of the blood-brain barrier (BBB), so that heterogeneous drug delivery into GBM may be a major contributor. In this context, preclinical studies are

JPET Fast Forward. Published on August 28, 2017 as DOI: 10.1124/jpet.117.243477
This article has not been copyedited and formatted. The final version may differ from this version.

needed to elucidate further details of underlying obstacles for effective drug delivery and treatment of brain tumors, such as GBM.

Treatment of GBM using targeted agents is complicated by extensive heterogeneity in the molecular and genetic makeup of the tumor (Phillips et al., 2006; Verhaak et al., 2010; Brennan et al., 2013; Parker et al., 2015), and the remarkable spatial heterogeneity in the permeability of the BBB (Jain et al., 2007). The use of selective tyrosine kinase inhibitors has not been useful to treat GBM. Coupled with heterogeneous drug distribution, dynamic interaction between oncogenic signaling pathways may contribute to the lack of efficacy of the highly targeted kinase inhibitors (Pazarentzos and Bivona, 2015). Upon selective inhibition of a molecular target, the targeted signaling pathway may adapt and activate an alternative “escape” signaling pathway that compensates for the “targeted” inhibition of a single driving oncogene (Pazarentzos and Bivona, 2015). For this reason, multi-kinase inhibitors are thought to delay such drug resistance mechanisms (Sierra and Tsao, 2011).

In addition, the tumor-induced inflammatory reactions in GBM often results in heterogeneous permeability of the BBB (Wolburg et al., 2012). The dramatic regional differences in drug delivery are possible in GBM where some tumor cells reside behind an intact BBB, while other cells are in regions where the BBB is “leaky” (Agarwal et al., 2011). Moreover, given the different tissue and tumor compositions at various anatomical sites (Devaud et al., 2014), the active (free) drug concentration could vary simply by differences in off-target binding and/or rapid clearance from certain tumor regions. Thus, design of an ideal molecularly-targeted agent for GBM should not only consider overcoming pathway-driven drug resistance, but also the delivery and bioavailability of therapeutic concentration to the infiltrating GBM cells.

Successful, predictive preclinical efficacy studies for the treatment of GBM must employ animal models that are representative of human disease, especially with respect to the heterogeneous breakdown of BBB in GBM (Jain et al., 2007) and the extensive abnormalities in molecular drivers of gliomagenesis (Crespo et al., 2015). Extensive tumor characterization has confirmed that the Mayo Clinic GBM PDX panel preserves the histomorphological and molecular features of the original patient tumor (Giannini et al., 2005). For this study, we have focused on GBM6, a well-characterized PDX in the Mayo Clinic GBM xenograft panel. This particular GBM line is resistant to temozolomide (TMZ) (Cen et al.,

JPET Fast Forward. Published on August 28, 2017 as DOI: 10.1124/jpet.117.243477
This article has not been copyedited and formatted. The final version may differ from this version.

2013) and a selective kinase inhibitor, erlotinib (ERL) (Sarkaria et al., 2007), when tumors are grown in an orthotopic location. In addition to restricted drug delivery to the brain, a proteomic analysis demonstrated that elevated expression of multiple receptor tyrosine kinases (RET and PDGFR-alpha) might also contribute to therapeutic resistance to a selective EGFR inhibitor (unpublished data). Therefore, the use of a multi-kinase inhibitor exhibiting potent activities against these molecular targets is warranted. We have identified ponatinib, an FDA approved treatment for chronic myeloid leukemia, as a candidate multi-targeted compound that has a compelling inhibitory potential against these targets in vitro at an IC_{50} of 0.2 nM against RET and 1.1 nM against PDGFR-alpha (European Medicines Agency, 2013). Therefore, ponatinib was selected be a suitable drug to examine how distribution and delivery may influence in vivo treatment efficacy for GBM.

Free (unbound) drug concentration at the site of action is thought to be the therapeutic or pharmacologically active concentration, while equilibrium exists between tissue-bound (total) and unbound (free) drugs. The free drug delivery and regional drug distribution have not been extensively studied in the preclinical GBM models. There have been no reports describing variable free drug fraction at different tumor regions and the consequent therapeutic implications in the treatment of brain tumors. In this study, in vivo efficacy of ponatinib, a multi-kinase inhibitor, was examined in GBM6 flank vs. orthotopic xenografts and subsequently, we evaluated free and total drug distribution of ponatinib in flank tumor and different regions of orthotopic GBM6 tumors. The data presented provides critical insights into the potential therapeutic implications of heterogeneity of free drug distribution in the brain tumors.

JPET Fast Forward. Published on August 28, 2017 as DOI: 10.1124/jpet.117.243477
This article has not been copyedited and formatted. The final version may differ from this version.

MATERIALS AND METHODS

Chemicals, reagents and supplies

Ponatinib (3-[2-(imidazo[1,2-b]pyridazin-3-yl)ethynyl]-4-methyl-N-{4-[(4-methylpiperazin-1-yl)methyl]-3-(trifluoromethyl)phenyl}benzamide) (>99% purity) was purchased from LC laboratories (Woburn, MA), imatinib methanesulfonate (4-[(4-methylpiperazin-1-yl)methyl]-N-[4-methyl-3-[(4-pyridin-3-ylpyrimidin-2-yl)amino]phenyl]benzamide methanesulfonate) (>99% purity) was purchased from LC Laboratories (Woburn, MA), and [$^{2}H_{8}$]-ponatinib (> 98% purity) was purchased from Alsachim SAS (Illkirch, France). Analytical-grade reagents were purchased from Fisher Scientific (Waltham, MA), and cell culture reagents were from Invitrogen (Carlsbad, CA). Parental pGIPZ lentiviral vector was sourced from Open Biosystems (GE Dharmacon, Lafayette, CO), HEK293T cells from ATCC (Manassas, VA), and pCDNA3.1(+)/Luc2=tdT from Addgene (Cambridge, MA). Rapid equilibrium dialysis (RED) device, comprised of a 96-well base plate and membrane inserts (8 kDa molecular weight cut-off cellulose dialysis membrane), was obtained from Thermo Fisher Scientific (Waltham, MA).

In vitro cell cultures and cytotoxicity assay

Short-term cultured human primary glioma GBM6 cells were previously characterized (Sarkaria et al., 2006; Sarkaria et al., 2007) and maintained through serial passages in the mouse via subcutaneous flank implantation in immune-deficient mice (Carlson et al., 2011). Short-term explant cultures were raised in serum-containing media (Dulbecco's modified Eagle's medium containing 10% fetal bovine serum and 1% penicillin/streptomycin) and were used for subcutaneous implantation (Carlson et al., 2011) and in vitro cytotoxicity assay. Explant cultures were plated on 96-well plates in triplicate and treated with ponatinib at varying concentrations. Following a 5-day treatment, the CyQUANT assay (Invitrogen) was performed as per the manufacturer's instructions.

Lentiviral vector and cell transduction

To enable precise dissection to separate tumor from surrounding brain tissues, GBM6 cells were genetically modified to express fluorescent protein. Briefly, a modified lentivirus vector pGIPZ-Luc2=tdT was developed by replacing turbo green fluorescent protein (GFP) tag of pGIPZ with a fusion of firefly

JPET Fast Forward. Published on August 28, 2017 as DOI: 10.1124/jpet.117.243477
This article has not been copyedited and formatted. The final version may differ from this version.

luciferase (Luc2) and tandem Tomato (tdT) red fluorescent protein excised from pcDNA3.1(+)/Luc2=tdT (Patel et al., 2010). Lentiviral particles were packaged in HEK293T cells and transduction to primary GBM6 cells was performed in the presence of 5 µg/mL polybrene (Millipore) as previously described (Gupta et al., 2014). Stable transductants expressing Luc2=tdT fusion gene (GBM6-Luc2=tdT) were selected in 5 µg/mL puromycin, and subsequently propagated as flank tumors.

Tumor-bearing animals

All studies employing animals were approved by the Institutional Animal Care and Use Committee, and all guidelines for the Care and Use of Laboratory Animals established by the U.S. National Institutes of Health (Bethesda, MD) were followed. All animals were housed in a standard 12-hour dark/light cycle with unlimited access to food and water.

Studies involving tumor implantation utilized female athymic nude mice (Hsd:athymic Nude-Foxn1^{nu}; Envigo, Indianapolis, IN) at the age of 6-7 weeks. Detailed procedures for PDX establishment were previously described (Carlson et al., 2011). Briefly, mice anesthetized using ketamine (100 mg/kg) and xylazine (10 mg/kg), and intracranially implanted with 3 µL of cell suspension (100,000 cells per µL) at 1 mm anterior and 2 mm lateral from the bregma. Subcutaneous flank-tumors were established by injecting the flank of athymic nude mice with 2 million cells suspended in 100 µL of Matrigel/phosphate buffered saline mixture. For tumor-tissue carving and imaging, orthotopic tumors were established from explant cultures of GBM6-Luc2=tdT xenograft line and allowed to grow for 3 weeks before extracting brain tissues and dissecting tumors.

Non-tumor-bearing animals

An equal number of female and male Friend leukemia virus strain B (FVB) wild-type mice (Taconic Biosciences, Inc., Germantown, NY) were utilized at the age of 8-14 weeks for all studies employing non-tumor-bearing animals. These animals were bred and maintained in the animal housing facility at the Academic Health Center, University of Minnesota.

In vivo efficacy of ponatinib in GBM6 xenograft animals

JPET Fast Forward. Published on August 28, 2017 as DOI: 10.1124/jpet.117.243477
This article has not been copyedited and formatted. The final version may differ from this version.

Mice with established flank tumors of approximately 200 mm^3 were randomized and treated with either placebo (*N* = 9-10; vehicle of 30% PEG 400 and 0.5% Tween 80) or ponatinib (*N* = 10; 30 mg/kg per day (O'Hare et al., 2009; Huang et al., 2010) via oral gavage until either the mice reached moribund state or the tumor volume exceeded 1500 mm^3. On Day 14 post-implantation, intracranial xenografts (*N* = 8-10*)* were randomized and treated with the same dosing regimen until moribund. Staff blinded to the treatment group measured flank tumors three times per week and observed the intracranial xenografts daily. Following the tumor implantation, the body weights of animals were monitored at least every other day until the moribund state. Animals were euthanized with carbon dioxide upon reaching each of the endpoints or other health issues noted.

Regional distribution of ponatinib in flank and intracranial tumor

Mice with established GBM6-Luc2=tdT tumor (flank tumors at least 200 mm^3 or orthotopic tumors at 14 days post-implantation) were randomized and treated with a single oral dose of placebo (group 1) or ponatinib (groups 2 and 3), followed by euthanasia at 1 hour (groups 1 and 2) or 6 hours (group 3) post dose. Plasma, flank tumor, thigh muscle (non-cancerous), and the brain tissues were collected as follows. Brain tissues extracted from orthotopically implanted animals were dissected under tdTomato goggles. The left hemisphere (without tumor) was first separated from the tumor-bearing right hemisphere. The right hemisphere was further carved to intracranial (IC) tumor core and peripheral region called hereafter the brain-around-tumor (BAT). Purity of tissue dissection was confirmed by ex vivo tissue imaging (IVIS Spectrum, PerkinElmer, Waltham, MA) as illustrated in Figure 4. Plasma, tumor, and various parts of brain were flash frozen on dry ice and stored at -80^oC until LC-MS/MS analysis or in vitro binding assay.

Plasma and brain pharmacokinetics of ponatinib

A single dose (30 mg/kg via oral gavage) of ponatinib was administered as an oral suspension (vehicle of 0.5% methylcellulose and 0.2% Tween 80) to FVB wild-type mice. The mice were euthanized by carbon dioxide inhalation at 0.5, 2, 4, 8, 12, 16, and 24 hours after oral administration (*N* = 4 at each time point). Blood was collected via cardiac puncture, transferred to heparinized tubes and stored on ice.

JPET Fast Forward. Published on August 28, 2017 as DOI: 10.1124/jpet.117.243477
This article has not been copyedited and formatted. The final version may differ from this version.

Brain was surgically extracted and rinsed in water. Plasma was separated by centrifuging the blood samples at 3500 rpm at 4^{o}C for 15 minutes. Both plasma and brain samples were stored at -80^{o}C until LC-MS/MS analysis.

In vitro binding assay: Determination of free (unbound) fraction of ponatinib

The free fraction in plasma, brain and tumor homogenate (flank tumor, intracranial tumor core, and BAT), and serum-containing media (Dulbecco's modified Eagle's medium containing 10% fetal bovine serum and 1% penicillin/streptomycin) were determined using a rapid equilibrium dialysis (RED) (Thermo Fisher Scientific) as per manufacturer's protocol with some modifications suggested in literature (Kalvass and Maurer, 2002; Friden et al., 2007). Briefly, the tissue homogenate in 3 volumes (w/v; 4-fold dilution) of phosphate buffered saline (PBS; pH 7.4) was prepared by mechanical homogenization (PowerGen 125; Thermo Fisher Scientific, Waltham, MA). Each matrix was spiked with ponatinib to a final concentration of 10 µM. The spiked matrix (300 µL) was loaded into the sample chamber and 500 µL of drug-free phosphate buffered saline (pH 7.4) into the corresponding buffer chamber in triplicate. The chambers, sealed with an adhesive lid, were incubated at 37^{o}C for 4 to 6 hours on an orbital shaker (300 rpm; ShelLab, Cornelius, OR). Samples after dialysis were stored at -80^{o}C until subsequent LC-MS/MS analysis.

Analytical LC-MS/MS analysis

Total drug concentration of ponatinib in various specimens was determined using reverse-phase liquid chromatography (Agilent model 1200 separation system; Agilent Technologies, Santa Clara, CA) interfaced with TSQ Quantum triple quadrupole mass spectrometer (Thermo Finnigan, San Jose, CA) by operating electrospray in positive ion mode and spray voltage at 4500 V. Brain samples were homogenized with 3 tissue volumes of 5% bovine serum albumin (g/v) solution using a homogenizer (PowerGen 125; Thermo Fisher Scientific, Waltham, MA). Ten volumes of 5% bovine serum albumin (g/v) solution was added to flank tumor, thigh muscle, and core and peripheral (BAT) regions of intracranial tumor, followed by homogenization using a tissue grinder (Kimble Kontes pellet pestle and cordless motor, Fisher Scientific, Waltham, MA). Liquid-liquid extraction was performed for 25 µL aliquot

of plasma or 50 µL aliquot of brain, thigh muscle, tumor or dialysis samples, by adding 75 ng of internal standard, 10 volumes of ice-cold ethyl acetate, and finally 5 volumes of 0.2 M sodium hydroxide (pH 13). Samples were mixed thoroughly by vortexing for 5 minutes, followed by centrifugation at 7500 rpm for 5 minutes (4^{o}C). Organic layer was dried under nitrogen and reconstituted by dissolving the content in 150 µL of mobile phase (acetonitrile and 20 mM ammonium acetate with 0.05% formic acid) and solution cleared by centrifugation at 14000 rpm for 5 minutes (4^{o}C). Five microliter of the sample was injected to the Zorbax XDB Eclipse C18 column (4.6 x 50 mm, 1.8 µm; Agilent Technologies) and subjected to liquid chromatography. Gradient elution with an internal standard imatinib was performed to separate analyte for the samples resulting from flank tumor distribution and pharmacokinetic studies. The initial condition of the mobile phase was comprised of 30% acetonitrile (B) and 70% 20-mM ammonium acetate with 0.05% formic acid (A; pH 4.5). Gradient elution was achieved as follows: Organic phase (B) was increased from 30% to 100% during the first 6 minutes, held at 100% for 2 minutes, decreased to 30% over 0.5 minutes and held at 30% for the remaining 7.5 minutes. The total run time was 16 minutes, and the flow rate was 0.25 mL/min. The retention times were 7.8 minutes for ponatinib and 4.8 minutes for imatinib, respectively. Mass-to-charge ratio (*m/z*) transitions were 533.1→260 for ponatinib and 494.3→394.1 for imatinib, respectively.

For all other study samples, a new isocratic method using a deuterated internal standard ([$^{2}H_{8}$]-ponatinib) was developed in order to reduce the total run time to 7 minutes. A mobile phase of 45% acetonitrile and 55% 20-mM ammonium acetate with 0.05% formic acid was eluted at a flow rate of 0.35 mL/min. The transition *m/z* 541→260 was monitored for [$^{2}H_{8}$]-ponatinib. The retention time was 3.1 minutes for ponatinib and its deuterated internal standard. For each of these LC-MS/MS methods, the calibration curve was sensitive and linear over the range of 0.4-2000 ng/mL (weighting factor of $1/Y^{2}$) with coefficient of variation of less than 15%. All of the measured concentrations were within the range of the calibration curve. Data acquisition and analysis were completed using Xcalibur software (version 2.0.7; Thermo Finnigan, San Jose, CA).

Calculations

JPET Fast Forward. Published on August 28, 2017 as DOI: 10.1124/jpet.117.243477
This article has not been copyedited and formatted. The final version may differ from this version.

Free fraction (fu) of ponatinib in the various tissue matrices was determined in vitro and calculated using the ratio of buffer concentration to matrix concentration. For matrices other than plasma, the calculation of free fraction accounted for dilution resulting from homogenate preparation (dilution factor, D = 4) as shown below (Kalvass and Maurer, 2002):

$$\text{Free fraction (fu)} = \frac{1/D}{\left(\left(\frac{1}{\text{fu,diluted}}\right)-1\right)+1/D} \quad \text{(Equation 1)}$$

A tissue partition coefficient (e.g., brain-to-plasma ratio or tumor-to-plasma ratio), or Kp was quantitated by the ratio of total tissue concentration to total plasma concentration. The unbound (free) derivative of Kp (Kp,uu) was determined as follows:

$$\text{Free tissue partition coefficient (Kp,uu)} = \text{Kp} \times \frac{\text{fu,tissue}}{\text{fu,plasma}} = \frac{\text{free tissue concentration}}{\text{free plasma concentration}} \quad \text{(Equation 2)}$$

where fu,tissue and fu,plasma represent the free fraction in the specified tissue and plasma, respectively. Total and free distribution advantage (DA_{total} and DA_{free}) to the tumor were calculated using the following equations:

$$\text{Total distribution advantage } (DA_{total}) = \frac{\text{Kp,flank tumor}}{\text{Kp,normal brain}} \text{ or } \frac{\text{Kp,IC tumor core}}{\text{Kp,BAT}} \quad \text{(Equation 3)}$$

$$\text{Free distribution advantage } (DA_{free}) = \frac{\text{Kp,uu,flank tumor}}{\text{Kp,uu,normal brain}} \text{ or } \frac{\text{Kp,uu,IC tumor core}}{\text{Kp,uu,BAT}} \quad \text{(Equation 4)}$$

Free drug concentrations were calculated by multiplying the total drug concentrations that were measured using LC-MS/MS with the corresponding fu values that were determined using in vitro binding assay (Liu et al., 2008). The total drug concentration-response curve resulting from in vitro cytotoxic assay was multiplied with the free fraction in serum-containing media (fu,media) in order to yield the free drug concentration-response curve. Total and free concentration-response curves were used to calculate total IC_{50} and free IC_{50}, respectively. The in vitro IC_{50} values were compared with the in vivo drug concentrations, assuming that the IC_{50} could serve as a hypothetical effective concentration to help explain the differences in response between flank tumor versus brain or different regions of intracranial tumor.

JPET Fast Forward. Published on August 28, 2017 as DOI: 10.1124/jpet.117.243477
This article has not been copyedited and formatted. The final version may differ from this version.

Pharmacokinetic data analysis

Plasma and brain concentration-over-time profiles from a single oral dose in FVB mice were analyzed using Phoenix WinNonlin version 6.4 (Certara USA, Inc., Princeton, NJ). The areas-under-the curve (AUCs) of brain and plasma concentrations were calculated by performing noncompartmental analysis (NCA). Log-linear trapezoidal integration was used to either the last time point ($AUC_{(0-t)}$) or time infinity ($AUC_{(0-\infty)}$) by including the extrapolated area beyond the last measured concentration. The area extrapolation was calculated by dividing the last measured concentration (C_{last}) with the terminal rate constant (λ) that describes the last three to five data points in the concentration profiles (Oberoi et al., 2013). The Phoenix's NCA module also reported other parameters/metrics, such as apparent clearance (CL/F), apparent volume of distribution (Vd/F), half-life, and Cmax. The brain-to-plasma ratio (Kp or Kp,uu) was calculated by the two methods: 1) the ratio of $AUC_{(0-\infty,brain)}$ to $AUC_{(0-\infty,plasma)}$ and 2) the ratio of the maximum brain concentration ($C_{max,brain}$) to the corresponding plasma concentration at that time point. A previous publication discussed that a transient steady-state occurs at the time of $C_{max,brain}$ ($T_{max,brain}$) as the rate of change of the brain concentration is zero at that time (Oberoi et al., 2013).

Statistical analysis

In vitro IC_{50} values were estimated by four-parameter nonlinear regression to characterize a log-transformed drug concentration-response curve. The mean estimated free fraction was compared between specimens using repeated unpaired two-sample *t* tests. Median survival and tumor progression beyond 1500 mm^3 (time to endpoint) were estimated by the Kaplan-Meier method and compared using the log-rank test. The Kp and Kp,uu values were compared to a hypothetical value of 1 (unity) by performing one-sample *t* tests. In addition, the total and free drug concentrations resulting from tumor distribution studies were compared with the total and free in vitro IC_{50} values using one-sample *t* tests. Data presentation and statistical tests were completed using GraphPad Prism (Version 6; GraphPad Software, La Jolla, California USA). All experimental data are presented as mean ± standard deviation (S.D.) or standard error of the mean (S.E.M). Based on our previous experience, sample sizes were estimated to obtain approximately 80% power to detect 50% difference between groups. In all cases, $P < 0.05$ was considered statistically significant.

JPET Fast Forward. Published on August 28, 2017 as DOI: 10.1124/jpet.117.243477
This article has not been copyedited and formatted. The final version may differ from this version.

RESULTS

In vitro efficacy of ponatinib in GBM6 tumor cells

The total IC_{50} value based on the experimental total drug concentration-response curve was 1.08 μM in GBM6 cell culture (Figure 1). The free fraction of ponatinib was determined in the serum-containing medium using rapid equilibrium dialysis. After adjustment to the free drug concentration-response profile, the free IC_{50} value was 0.032 μM (Figure 1).

In vivo efficacy of ponatinib in flank and orthotopic GBM6 xenografts

The efficacy of ponatinib was initially evaluated in flank GBM6 tumor models to avoid the potential confounding influence of drug delivery across the BBB. Ponatinib (30 mg/kg per day via oral gavage) significantly prolonged the time to the tumor growth endpoint (progression beyond 1500 mm^3) in GBM6 flank xenografts (37 vs. 28 days, **P* = 0.0018; Figure 2A). Results from this study in the flank tumor model suggested that ponatinib was modestly effective in GBM model in vivo. We then tested efficacy of the same ponatinib regimen in orthotopic model. Interestingly, unlike the tumor stasis observed in flank xenografts, ponatinib was inefficacious with improving the median survival (37.5 vs. 35 days, *P* = 0.42; Figure 2B) in the orthotopic model. These results indicate that ponatinib was effective in heterotopic but not in orthotopic GBM6 PDX tumors. The ponatinib treatment did not result in a significant weight loss in the flank and orthotopic GBM6 xenografts (Supplemental Figure 1). The body weights stayed within 20% of the baseline value until the day of euthanasia, regardless of the treatment (placebo or ponatinib) group.

Brain distribution of ponatinib

The brain and plasma concentrations, and brain-to-plasma ratio profiles after a single oral dose (30 mg/kg) of ponatinib in FVB wild-type, GBM6 flank and intracranial xenografts are presented in Figure 3. The brain and plasma concentrations, and brain-to-plasma ratios estimated in tumor-bearing animals at 1 and 6 hour time points agreed with the time-course profile determined in FVB mice, indicating a lack of significant difference in the concentrations and estimates of brain-to-plasma ratios regardless of the mouse strain. As shown in Figure 3A, the total drug concentrations were lower in the brain than plasma up to 12 hours post dose. However, the total brain drug concentrations were similar to the total plasma

concentrations during the last two time points (16 and 24 hours post dose). The maximum concentration of ponatinib occurred at 2 hours post dose both in the brain and plasma. The apparent volume of distribution (Vd/F) was 17.6 liters/kg, and the apparent clearance (CL/F) was 46.6 mL/min/kg, as shown in Table 1. The Kp values determined from the AUC ratios ($AUC_{(0-\infty,brain)}/AUC_{(0-\infty,plasma)}$ or $AUC_{(0-t,brain)}/AUC_{(0-t,plasma)}$) were about 0.8, and the value was similar regardless of using $AUC_{(0-t)}$ or $AUC_{(0-\infty)}$ given the low percent (< 6%) extrapolated from the last measured time point to infinity for the calculation of AUC. The transient steady-state brain-to-plasma ratio (Kp) was 0.87, which closely matched the AUC ratio based Kp values. In Figure 3B, the free plasma concentrations were consistently greater than the free brain concentrations throughout all time points after administration of a single oral dose of ponatinib. The Kp,uu values based on $AUC_{(0-\infty)}$ or transient steady-state concentrations were about 0.1, which was considerably below unity (1) (Table 1). Such Kp,uu values indicate restricted brain penetration of ponatinib across the BBB. Figure 3C shows the time course of instantaneous Kp and Kp,uu values. The Kp values increased up to 2 hours post dose and stayed consistently around 1 throughout the rest of time points. However, the Kp,uu values stayed below 1 throughout all time points.

Drug binding at various tissue sites

An incubation time of 4 hours was adequate to reach equilibrium between the buffer and sample chambers during the rapid equilibrium dialysis (RED) experiment. We observed that there was no difference in the estimated free fraction (fu) after 4 hours versus 6 hours of incubation, indicating that equilibrium had been reached at 4 hours. Due to the limited tissue quantity available of intracranial tumor, the free fraction of pontatinib in the intracranial tumor was estimated using an incubation time of 4 hours.

The free fraction of ponatinib in different regions of tumor-bearing brain was evaluated, using the specimens collected from tdTomato-guided dissection of tumor regions as illustrated in Figure 4. The data resulting from the in vitro binding assay are displayed in Figure 5 and Table 2. All specimens had a free fraction of less than 1%. Notably, the free fraction in plasma was about 10-fold higher than normal brain (*P = 0.0071). The BAT showed the similar free fraction as normal brain (P = 0.24). However, the intracranial tumor core showed a 5-fold higher free fraction than the BAT (*P = 0.032), suggesting

heterogeneous drug-tissue binding across different regions of the intracranial tumor-bearing brain. Interestingly, the free fraction was similar between flank tumor and intracranial tumor core (P = 0.42).

Site-differential drug distribution

Total and free drug distribution in different regions of tumor-bearing brain was also examined, using the specimens collected from tdTomato-guided dissection of tumor regions as illustrated in Figure 4. Total and free drug concentrations resulting from the tumor-site specific drug distribution studies are presented in Figure 6 and Supplemental Table 1. In GBM6 flank xenografts, there were greater total and free drug exposure in flank tumor than the non-tumor bearing (normal) brain at two different time points. The total and free concentrations were consistently higher in flank tumor compared to normal brain at both 1 and 6 hours, respectively, after administration of a single dose of ponatinib (30 mg/kg) to mice with flank xenografts (Figures 6A and 6B). The total concentration of ponatinib in non-cancerous thigh muscle was significantly higher than in normal brain at both 1 and 6 hour time points (Figure 6A). At the 6 hour time point, however, the total concentration in the non-cancerous thigh muscle was lower than the flank tumor, indicating that ponatinib distribution is different between the cancerous and non-cancerous peripheral tissues, as may be anticipated by anatomical differences in vessel structure and function related to tumor-induced angiogenic processes. The total and free tissue partition coefficients (Kp and Kp,uu) were at least 4-fold higher in flank tumor than the normal brain (Figures 7A and 7B, and Supplemental Table 1) as reflected in the DA_{total} and DA_{free} values, respectively, demonstrating limited drug delivery to the brain compared to flank tumor. The Kp value was greater than 1 (*circa* 2.6 to 8.8) in the flank tumor and non-cancerous thigh muscle (*circa* 2.7 to 4.0), but less than or equal to 1 in the normal brain (*circa* 0.6 to 1.2), at both time points (1 and 6 hours post dose). The Kp,uu value was consistently and significantly less than 1 for normal brain at both time points, whereas the Kp,uu value in the flank tumor equaled or exceeded unity (1) (Figure 7B).

In GBM6 intracranial xenografts, regional differences in total and free drug concentrations were observed between the intracranial tumor core and BAT. The total and free drug concentrations were consistently higher in tumor core versus BAT after 1 and 6 hours, respectively, of ponatinib treatment (Figures 6C and 6D, and Supplemental Table 1). The intracranial tumor core had at least 3-fold higher

JPET Fast Forward. Published on August 28, 2017 as DOI: 10.1124/jpet.117.243477
This article has not been copyedited and formatted. The final version may differ from this version.

total and free tissue partition coefficients (Kp and Kp,uu) than BAT, at both time points (Figures 7C and 7D, and Supplemental Table 1). As reflected in the DA_{total} and DA_{free} values in these regions, the growing edge of intracranial tumor (brain-around-tumor, BAT) has relatively impeded drug accumulation compared to the necrotic core of intracranial tumor.

The total and free drug concentrations resulting from drug distribution studies were compared with its respective IC_{50} values. The total concentrations in flank tumor exceeded the total IC_{50} value at least by 2.5-fold at 1 and 6 hours, respectively, after ponatinib treatment whereas the normal brain did not (Figure 6A and Supplemental Table 1). These data suggest that drug distribution to normal brain is disadvantaged. In the intracranial xenografts, the total drug concentration in the intracranial tumor core exceeded the total IC_{50} value, at both time points, but did not in the BAT (Figure 6C and Supplemental Table 1), indicating regional differences in drug accumulation in the intracranial tumor. The relative differences in drug concentrations and the total IC_{50} value in the tissue sites were consistent with the contrasted efficacy between flank versus orthotopic models. However, in vitro free IC_{50} was not reached even with the maximum tolerated dose of ponatinib (30 mg/kg per day) (Figures 6B and 6D).

DISCUSSION

We have previously reported differences in the distribution of small molecule tyrosine kinase inhibitors between flank and orthotopic tumor sites, which resulted in variable treatment efficacy in PDX GBM models (Parrish et al., 2015; Pokorny et al., 2015). These studies showed the link between limited drug distribution to the brain and lack of efficacy in orthotopic tumors. The current study showed a similar finding for ponatinib, and further indicated that various regions of the brain and brain tumor, i.e., the normal brain (contralateral hemisphere) and the invasive rim of an intracranial tumor (brain-around-tumor, BAT), have variable and limited total (i.e., free and bound) drug distribution. Importantly, these data also revealed that these intracranial regions had lower levels of free drug exposure compared to the flank tumor, in spite of a relatively high total brain-to-plasma partition coefficient (Kp) near unity.

The free drug concentration in plasma is considered to be a driving force for distributional processes, including distribution to the brain, according to the free drug hypothesis (Dubey et al., 1989; Hammarlund-Udenaes et al., 2008; de Lange, 2013). Brain drug penetration is modulated by the blood-

brain barrier (BBB), where tight junctions prevent paracellular drug transport and efflux transporters reduce drug accumulation in the brain (Abbott et al., 2006). However, this vascular barrier is quite different in the peripheral vasculature, and greater drug penetration to a flank tumor versus intracranial tumor for a tyrosine kinase inhibitor has been reported (Parrish et al., 2015). If the AUC of free drug in the brain and plasma were equal, the observed Kp,uu would be 1, indicating the absence of net transporter-mediated drug flux and that passive diffusion is possibly the only transport process at the BBB. This situation may result in similar free brain concentration and free plasma concentration profiles. In the current study, the Kp,uu value for ponatinib, however, was significantly below 1 in the normal brain and the invasive rim (BAT) of intracranial tumor (Figure 7), indicating that active efflux transport modulates the ponatinib accumulation in the brain. It is important to note that the assessment of brain penetration using a total brain-to-plasma ratio (Kp) can be misleading for a compound, such as ponatinib, because the Kp value does not account for free drug concentration ratios across the BBB, where efflux transporters can lead to a greater clearance out of, than into, the brain. These free plasma and brain concentration data (Figure 3), and the resultant Kp,uu, suggest that efflux transport strongly influences ponatinib brain penetration. This finding was not surprising, since we have previously shown that ponatinib is a substrate of the two major efflux transporters in the BBB, breast cancer resistance protein (Bcrp) and p-glycoprotein (P-gp/Mdr1). In studies examining the brain distribution of ponatinib in wild-type and transporter deficient mice, the brain-to-plasma Kp value for total drug was 18-fold higher in the *Mdr1a/b(-/-)Bcrp1(-/-)* mice lacking Bcrp and P-gp compared to wild-type (Laramy et al., 2015; Laramy et al., 2016).

The extent of free drug fraction at the site of action is anticipated to differ depending on the tissue composition. The study by Ha et al. demonstrated that the lipid composition differs between tumor tissues obtained from flank and orthotopic implantation in NOD.CB17-*Prkdc*^{scid}/J (NOD/Scid) mice, based on a lipidomic analysis for two human GBM xenograft lines (GBM10 and GBM43 from the Mayo Clinic GBM PDX panel) (Ha et al., 2007). This finding suggests that even for the same tumor xenograft, different tissue-dependent microenvironments can result in widely varying free fractions of a drug. Our in vitro binding assay demonstrated differences in the free drug fraction between the two tumor sites, where the free fraction was about 4-fold higher in the flank tumor environment than the invasive growing edge of

the intracranial tumor environment. Our finding is consistent with the theory that different tissue compositions can influence the free fraction and hence, free drug exposure at the site of action (tumor). If the brain-to-plasma partitioning of total drug (in the case of ponatinib, Kp ~ 1) is the only parameter used for the assessment of brain penetration, it is possible to erroneously conclude that drug exposure is not an issue in the lack of efficacy in orthotopic GBM. The current study showed that the free fraction of ponatinib was about 10-fold lower in the invasive BAT region (and normal brain) than plasma. Solely due to the different free fraction between plasma and brain, the Kp,uu between brain and plasma became 0.1; while the Kp value reached unity. The Kp,uu below unity was also expected because ponatinib is a substrate of the two major efflux transporters in the BBB (Laramy et al., 2015; Laramy et al., 2016). The Kp,uu between flank tumor (or intracranial tumor core) and plasma equaled or exceeded unity at 1 and 6 hours post dose, whereas the Kp,uu stayed below unity in the growing edge of the tumor (BAT), i.e., the desired site of action. The compromised free drug exposure in the brain compared to flank tumor may account for the differences in efficacy between the flank and orthotopic tumors. This may be an important consideration when conducting in vivo screening for efficacy of anti-tumor therapies for brain tumors. The tissue-dependent composition and binding highlight that the tumor implantation to two sites (e.g., flank and orthotopic) can not only allow exploration of the influence of different tumor sites on efficacy testing, but also drug delivery issues that have therapeutic consequences, such as a different free fraction in various tumor microenvironments.

The use of heterotopic and orthotopic GBM models within a single study was useful in investigating differences in free fraction and site-dependent drug delivery. A greater therapeutic advantage, in terms of free drug exposure, was observed in flank tumor than orthotopic tumor, in part, because the efflux or blood-tissue barrier is absent in the flank tumor unlike the orthotopic tumor. Figure 8A shows a hypothetical schematic of the equilibration of free (unbound) drugs across different tissue compartments, including blood, flank and orthotopic tumors. Orthotopic GBM tumor models have distinctive disadvantages to effective therapy because of the heterogeneity in the BBB vasculature. Angiogenesis, often accompanying dissemination of glioblastoma invasion, causes a focal disruption of the BBB (Jain et al., 2007; Claes et al., 2008). As a result, the BBB vasculature is relatively leakier in the core region in contrast to the brain parenchyma that is farther away from the necrotic tumor core (Youland

et al., 2013) (Figure 8B). The BAT, or the growing edge region of intracranial tumor, is the therapeutically critical area that requires "adequate" free drug exposure, in order to enhance efficacy of invasive GBM. This particular area is not visualized by contrast-enhanced imaging and thus not removed by the imaging-guided surgical resection of the necrotic core (Agarwal et al., 2011; Youland et al., 2013). The lower Kp,uu and free drug concentration of ponatinib in the BAT than the intracranial tumor core suggest that intact BBB may reduce the penetration of ponatinib to the growing edge and thus allow GBM invasion throughout the rest of the brain (Figure 8C).

The present study showed that regional differences in total and free drug exposure in the brain or across different regions of an intracranial tumor may negatively affect efficacy in an orthotopic model. The free concentration of ponatinib was lower in the invasive rim of intracranial tumor and normal brain compared to flank tumor and brain tumor core. The assessment of Kp,uu also revealed the potential influence of transporter-mediated drug efflux on ponatinib CNS delivery, confirmed by transporter-deficient mouse models. The free fraction of ponatinib was variable at various tumor sites, suggesting that differences in the tumor or tissue microenvironment, i.e., the composition of a binding matrix, can influence efficacy through spatial heterogeneity in active (free) drug exposure.

A limitation of the present study is that the in vitro IC_{50} value was notably above the in vivo free concentration of ponatinib in flank tumor, leading to in vitro-in vivo discrepancies in predicting the site-dependent efficacy. A possible explanation is that the estimation of free fraction in the serum-containing media (used for scaling total IC_{50} to free IC_{50}) might have been overestimated, perhaps, due to other non-specific binding (e.g., cell culture apparatus) and complex in vivo processes (e.g., metabolism and other cellular processes) that can further sequester free drug. It is also possible that inclusion of additional data points in the response region of the drug concentration-time curve could have improved the estimation of the IC_{50}.

In conclusion, this study showed that there was a significant difference in the flank versus orthotopic efficacy of the multi-targeted kinase inhibitor ponatinib against a GBM PDX that exhibited resistance to standard therapy. Despite the apparent high brain penetration of ponatinib based on the total drug concentrations and AUC ratio (Kp), the AUC ratio of free drug (Kp,uu) between brain and plasma was significantly less than unity when free fractions were used to determine the partitioning of

free drug. The Kp,uu of brain below unity can indicate a net efflux process out of the brain. Importantly, this free Kp,uu varied amongst tumor sites (brain vs flank) and even within a tumor site (core vs brain-around-tumor, BAT). The tumor microenvironment and site-dependent variability in drug-tissue binding may account for the lower, free (active) drug exposure in the BAT, the critical site of action for effective GBM treatment.

ACKNOWLEDGMENTS

The authors thank Jim Fisher, Clinical Pharmacology Analytical Laboratory, University of Minnesota, for his support in the development of the LC-MS/MS assay.

AUTHORSHIP CONTRIBUTIONS

Participated in research design: Laramy, Gupta, Ma, Parrish, Sarkaria, Elmquist

Conducted experiments: Laramy, Kim, Parrish, Gupta, Mladek, Bakken, Carlson

Conducted data analysis: Laramy, Parrish, Sarkaria, Elmquist

Contributed to LC-MS/MS assay development: Laramy, Zhang

Wrote or contributed to the writing of the manuscript: Laramy, Parrish, Kim, Gupta, Sarkaria, Elmquist

REFERENCES

Abbott NJ, Ronnback L and Hansson E (2006) Astrocyte-endothelial interactions at the blood-brain barrier. *Nat Rev Neurosci* **7**:41-53.

Agarwal S, Sane R, Oberoi R, Ohlfest JR and Elmquist WF (2011) Delivery of molecularly targeted therapy to malignant glioma, a disease of the whole brain. *Expert Rev Mol Med* **13**:e17.

Brennan CW, Verhaak RG, McKenna A, Campos B, Noushmehr H, Salama SR, Zheng S, Chakravarty D, Sanborn JZ, Berman SH, Beroukhim R, Bernard B, Wu CJ, Genovese G, Shmulevich I, Barnholtz-Sloan J, Zou L, Vegesna R, Shukla SA, Ciriello G, Yung WK, Zhang W, Sougnez C, Mikkelsen T, Aldape K, Bigner DD, Van Meir EG, Prados M, Sloan A, Black KL, Eschbacher J, Finocchiaro G, Friedman W, Andrews DW, Guha A, Iacocca M, O'Neill BP, Foltz G, Myers J, Weisenberger DJ, Penny R, Kucherlapati R, Perou CM, Hayes DN, Gibbs R, Marra M, Mills GB, Lander E, Spellman P, Wilson R, Sander C, Weinstein J, Meyerson M, Gabriel S, Laird PW, Haussler D, Getz G, Chin L and Network TR (2013) The somatic genomic landscape of glioblastoma. *Cell* **155**:462-477.

Carlson BL, Pokorny JL, Schroeder MA and Sarkaria JN (2011) Establishment, maintenance and in vitro and in vivo applications of primary human glioblastoma multiforme (GBM) xenograft models for translational biology studies and drug discovery. *Curr Protoc Pharmacol* **Chapter 14**:Unit 14 16.

Cen L, Carlson BL, Pokorny JL, Mladek AC, Grogan PT, Schroeder MA, Decker PA, Anderson SK, Giannini C, Wu W, Ballman KV, Kitange GJ and Sarkaria JN (2013) Efficacy of protracted temozolomide dosing is limited in MGMT unmethylated GBM xenograft models. *Neuro Oncol* **15**:735-746.

Claes A, Wesseling P, Jeuken J, Maass C, Heerschap A and Leenders WP (2008) Antiangiogenic compounds interfere with chemotherapy of brain tumors due to vessel normalization. *Mol Cancer Ther* **7**:71-78.

Crespo I, Vital AL, Gonzalez-Tablas M, Patino Mdel C, Otero A, Lopes MC, de Oliveira C, Domingues P, Orfao A and Tabernero MD (2015) Molecular and Genomic Alterations in Glioblastoma Multiforme. *Am J Pathol* **185**:1820-1833.

de Lange EC (2013) The mastermind approach to CNS drug therapy: translational prediction of human brain distribution, target site kinetics, and therapeutic effects. *Fluids Barriers CNS* **10**:12.

Devaud C, Westwood JA, John LB, Flynn JK, Paquet-Fifield S, Duong CP, Yong CS, Pegram HJ, Stacker SA, Achen MG, Stewart TJ, Snyder LA, Teng MW, Smyth MJ, Darcy PK and Kershaw MH (2014) Tissues in different anatomical sites can sculpt and vary the tumor microenvironment to affect responses to therapy. *Mol Ther* **22**:18-27.

Dubey RK, McAllister CB, Inoue M and Wilkinson GR (1989) Plasma binding and transport of diazepam across the blood-brain barrier. No evidence for in vivo enhanced dissociation. *J Clin Invest* **84**:1155-1159.

European Medicines Agency (2013). *Iclusig: CHMP assessment report (EMA/CHMP/220290/2013). Committee for Medicinal Products for Human Use*, CHMP, London.

Friden M, Gupta A, Antonsson M, Bredberg U and Hammarlund-Udenaes M (2007) In vitro methods for estimating unbound drug concentrations in the brain interstitial and intracellular fluids. *Drug Metab Dispos* **35**:1711-1719.

Giannini C, Sarkaria JN, Saito A, Uhm JH, Galanis E, Carlson BL, Schroeder MA and James CD (2005) Patient tumor EGFR and PDGFRA gene amplifications retained in an invasive intracranial xenograft model of glioblastoma multiforme. *Neuro Oncol* **7**:164-176.

Gupta SK, Mladek AC, Carlson BL, Boakye-Agyeman F, Bakken KK, Kizilbash SH, Schroeder MA, Reid J and Sarkaria JN (2014) Discordant in vitro and in vivo chemopotentiating effects of the PARP inhibitor veliparib in temozolomide-sensitive versus -resistant glioblastoma multiforme xenografts. *Clin Cancer Res* **20**:3730-3741.

Ha SJ, Showalter G, Cai S, Wang H, Liu WM, Cohen-Gadol AA, Sarkaria JN, Rickus J, Springer J, Adamec J, Pollok KE and Clase KL (2007) Lipidomic Analysis of Glioblastoma Multiforme Using Mass Spectrometry. *Anal Chem* **79**:8423–8430.

Hammarlund-Udenaes M, Friden M, Syvanen S and Gupta A (2008) On the rate and extent of drug delivery to the brain. *Pharm Res* **25**:1737-1750.

Huang WS, Metcalf CA, Sundaramoorthi R, Wang Y, Zou D, Thomas RM, Zhu X, Cai L, Wen D, Liu S, Romero J, Qi J, Chen I, Banda G, Lentini SP, Das S, Xu Q, Keats J, Wang F, Wardwell S, Ning

Y, Snodgrass JT, Broudy MI, Russian K, Zhou T, Commodore L, Narasimhan NI, Mohemmad QK, Iuliucci J, Rivera VM, Dalgarno DC, Sawyer TK, Clackson T and Shakespeare WC (2010) Discovery of 3-[2-(imidazo[1,2-b]pyridazin-3-yl)ethynyl]-4-methyl-N-{4-[(4-methylpiperazin-1-yl)methyl]-3-(trifluoromethyl)phenyl}benzamide (AP24534), a potent, orally active pan-inhibitor of breakpoint cluster region-abelson (BCR-ABL) kinase including the T315I gatekeeper mutant. *J Med Chem* **53**:4701-4719.

Jain RK, di Tomaso E, Duda DG, Loeffler JS, Sorensen AG and Batchelor TT (2007) Angiogenesis in brain tumours. *Nat Rev Neurosci* **8**:610-622.

Kalvass JC and Maurer TS (2002) Influence of nonspecific brain and plasma binding on CNS exposure: implications for rational drug discovery. *Biopharm Drug Dispos* **23**:327-338.

Laramy JK, Parrish KE and Elmquist WF (2016) Influence of Efflux Transporters on the Pharmacokinetics and Biodistribution of Ponatinib, a Multi-kinase Inhibitor. *Poster presentation at the 2016 American Association of Pharmaceutical Scientists (AAPS) Annual Meeting and Exposition*; November 13-17, 2016; Colorado, Denver. Poster 07T0400.

Laramy JK, Parrish KE, Zhang S, Bakken K, Carlson BL, Mladek A, Ma D, Sarkaria J and Elmquist W (2015) Brain Distribution of Ponatinib, a Multi-kinase Inhibitor: Implications for the Treatment of Malignant Brain Tumors. *Poster presentation at the 2015 American Association of Pharmaceutical Scientists (AAPS) Annual Meeting and Exposition*; October 25-29, 2015; Orlando, Florida. Poster W4339.

Liu X, Chen C and Smith BJ (2008) Progress in brain penetration evaluation in drug discovery and development. *J Pharmacol Exp Ther* **325**:349-356.

Minniti G, Muni R, Lanzetta G, Marchetti P and Enrici RM (2009) Chemotherapy for glioblastoma: current treatment and future perspectives for cytotoxic and targeted agents. *Anticancer Res* **29**:5171-5184.

O'Hare T, Shakespeare WC, Zhu X, Eide CA, Rivera VM, Wang F, Adrian LT, Zhou T, Huang WS, Xu Q, Metcalf CA, 3rd, Tyner JW, Loriaux MM, Corbin AS, Wardwell S, Ning Y, Keats JA, Wang Y, Sundaramoorthi R, Thomas M, Zhou D, Snodgrass J, Commodore L, Sawyer TK, Dalgarno DC, Deininger MW, Druker BJ and Clackson T (2009) AP24534, a pan-BCR-ABL inhibitor for chronic

myeloid leukemia, potently inhibits the T315I mutant and overcomes mutation-based resistance. *Cancer Cell* **16**:401-412.

Oberoi RK, Mittapalli RK and Elmquist WF (2013) Pharmacokinetic assessment of efflux transport in sunitinib distribution to the brain. *J Pharmacol Exp Ther* **347**:755-764.

Oberoi RK, Parrish KE, Sio TT, Mittapalli RK, Elmquist WF and Sarkaria JN (2016) Strategies to improve delivery of anticancer drugs across the blood-brain barrier to treat glioblastoma. *Neuro Oncol* **18**:27-36.

Ostrom QT, Gittleman H, Xu J, Kromer C, Wolinsky Y, Kruchko C and Barnholtz-Sloan JS (2016) CBTRUS Statistical Report: Primary Brain and Other Central Nervous System Tumors Diagnosed in the United States in 2009-2013. *Neuro Oncol* **18**:v1-v75.

Parker NR, Khong P, Parkinson JF, Howell VM and Wheeler HR (2015) Molecular heterogeneity in glioblastoma: potential clinical implications. *Front Oncol* **5**:55.

Parrish KE, Pokorny J, Mittapalli RK, Bakken K, Sarkaria JN and Elmquist WF (2015) Efflux transporters at the blood-brain barrier limit delivery and efficacy of cyclin-dependent kinase 4/6 inhibitor palbociclib (PD-0332991) in an orthotopic brain tumor model. *J Pharmacol Exp Ther* **355**:264-271.

Patel MR, Chang YF, Chen IY, Bachmann MH, Yan X, Contag CH and Gambhir SS (2010) Longitudinal, noninvasive imaging of T-cell effector function and proliferation in living subjects. *Cancer Res* **70**:10141-10149.

Pazarentzos E and Bivona TG (2015) Adaptive stress signaling in targeted cancer therapy resistance. *Oncogene* **34**:5599-5606.

Phillips HS, Kharbanda S, Chen R, Forrest WF, Soriano RH, Wu TD, Misra A, Nigro JM, Colman H, Soroceanu L, Williams PM, Modrusan Z, Feuerstein BG and Aldape K (2006) Molecular subclasses of high-grade glioma predict prognosis, delineate a pattern of disease progression, and resemble stages in neurogenesis. *Cancer Cell* **9**:157-173.

Pokorny JL, Calligaris D, Gupta SK, Iyekegbe DO, Jr., Mueller D, Bakken KK, Carlson BL, Schroeder MA, Evans DL, Lou Z, Decker PA, Eckel-Passow JE, Pucci V, Ma B, Shumway SD, Elmquist WF, Agar NY and Sarkaria JN (2015) The Efficacy of the Wee1 Inhibitor MK-1775 Combined with

Temozolomide Is Limited by Heterogeneous Distribution across the Blood-Brain Barrier in Glioblastoma. *Clin Cancer Res* **21**:1916-1924.

Sarkaria JN, Carlson BL, Schroeder MA, Grogan P, Brown PD, Giannini C, Ballman KV, Kitange GJ, Guha A, Pandita A and James CD (2006) Use of an orthotopic xenograft model for assessing the effect of epidermal growth factor receptor amplification on glioblastoma radiation response. *Clin Cancer Res* **12**:2264-2271.

Sarkaria JN, Yang L, Grogan PT, Kitange GJ, Carlson BL, Schroeder MA, Galanis E, Giannini C, Wu W, Dinca EB and James CD (2007) Identification of molecular characteristics correlated with glioblastoma sensitivity to EGFR kinase inhibition through use of an intracranial xenograft test panel. *Mol Cancer Ther* **6**:1167-1174.

Sierra JR and Tsao MS (2011) c-MET as a potential therapeutic target and biomarker in cancer. *Ther Adv Med Oncol* **3**:S21-35.

Verhaak RG, Hoadley KA, Purdom E, Wang V, Qi Y, Wilkerson MD, Miller CR, Ding L, Golub T, Mesirov JP, Alexe G, Lawrence M, O'Kelly M, Tamayo P, Weir BA, Gabriel S, Winckler W, Gupta S, Jakkula L, Feiler HS, Hodgson JG, James CD, Sarkaria JN, Brennan C, Kahn A, Spellman PT, Wilson RK, Speed TP, Gray JW, Meyerson M, Getz G, Perou CM, Hayes DN and Cancer Genome Atlas Research N (2010) Integrated genomic analysis identifies clinically relevant subtypes of glioblastoma characterized by abnormalities in PDGFRA, IDH1, EGFR, and NF1. *Cancer Cell* **17**:98-110.

Wolburg H, Noell S, Fallier-Becker P, Mack AF and Wolburg-Buchholz K (2012) The disturbed blood-brain barrier in human glioblastoma. *Mol Aspects Med* **33**:579-589.

Youland RS, Kitange GJ, Peterson TE, Pafundi DH, Ramiscal JA, Pokorny JL, Giannini C, Laack NN, Parney IF, Lowe VJ, Brinkmann DH and Sarkaria JN (2013) The role of LAT1 in (18)F-DOPA uptake in malignant gliomas. *J Neurooncol* **111**:11-18.

FOOTNOTES

This work was supported by the National Institutes of Health [Grants RO1 CA138437, RO1 NS077921, U54 CA210180, and P50 CA108960]. Janice K. Laramy was supported by the Edward G. Rippie, Rory P. Remmel and Cheryl L. Zimmerman in Drug Metabolism and Pharmacokinetics, and American Foundation for Pharmaceutical Education Pre-Doctoral Fellowships.

JPET Fast Forward. Published on August 28, 2017 as DOI: 10.1124/jpet.117.243477
This article has not been copyedited and formatted. The final version may differ from this version.

LEGENDS FOR FIGURES

Figure 1. In vitro efficacy of ponatinib: Growth curve showing effect of various concentrations of ponatinib on GBM6 cells in vitro as determined by CyQUANT assay. The IC_{50} value resulting from response curves for the experimental total drug concentration (solid line, presented as mean ± standard error of the mean (S.E.M); *N* = 3 in triplicate) or free drug concentration (dotted line, determined using the measured free fraction in serum-containing media). The total and free IC_{50} values were 1.08 μM and 0.032 μM, respectively, in GBM6 cell culture.

Figure 2. Evaluation of in vivo efficacy of ponatinib (30 mg/kg per day) in GBM6 xenografts. (A) Kaplan-Meier curves for GBM6 flank xenografts (*N* = 9-10) with the end point of tumor size exceeding 1500 mm^3 (* *P* < 0.05). (B) Kaplan-Meier curves for GBM6 intracranial xenografts (*N* = 8-10) showing no difference in survival between placebo and ponatinib groups (*P* > 0.05, *N.S.,* not significant).

Figure 3. Pharmacokinetic profiles after administration of a single oral dose (30 mg/kg) of ponatinib in FVB wild-type mice, GBM6 flank and intracranial xenografts. (A) Total brain (dotted line with circle) and plasma (solid line with square) concentration-over-time curves. (B) Free brain (dotted line with circle) and plasma (solid line with square) concentration-over-time curves. (C) Total brain-to-plasma ratio (Kp; solid line with triangle) and free brain-to-plasma ratio (Kp,uu; dotted line with upside-down triangle). Data are presented as mean ± standard deviation (S.D.). The data in FVB wild-type mice are displayed in black color, those in GBM6 flank xenografts in red, and GBM6 intracranial xenografts in blue.

Figure 4. A representative image illustrating how different regions of tumor-bearing brain were dissected after visualizing the tumor with ex vivo imaging. The tumor cells expressing red fluorescence (tdTomato) were injected into the right hemisphere. The tumor center with the highest fluorescent signal was defined as the core, the surrounding brain tissue as the brain-around-tumor (BAT), and the contralateral hemisphere as the normal brain. (A) Brain without tumor. (B) Brain with tumor. (C) Separation of tumor and brain. The letters: L = left hemisphere, R = right hemisphere, T= tumor core, BAT = brain-around-

tumor, N = normal brain, line bar = 1 cm, color scale on the right was adjusted to represent each picture shown. The green dotted lines outline each of the intracranial regions.

Figure 5. Free fraction (fu) values determined from in vitro rapid equilibrium dialysis (RED) experiment after 4-hour incubation in triplicate. Two-sample *t* test was performed to compare plasma versus normal brain (* $P < 0.05$), normal brain versus brain around intracranial tumor (BAT) ($P > 0.05$; *N.S.,* not significant), intracranial tumor core (IC tumor core) versus BAT (* $P < 0.05$), and IC core versus flank tumor ($P > 0.05$; *N.S.,* not significant). Data are presented as mean ± standard deviation (S.D.).

Figure 6. Concentrations of ponatinib at 1 and 6 hours after administration of a single oral dose (30 mg/kg) of ponatinib in GBM6 flank and intracranial xenograft mice in tumor distribution studies. (A) Total drug concentration in plasma, normal brain, flank tumor, and thigh muscle (non-cancerous) in flank xenograft mice ($N = 4$-6). (B) Free drug concentration in plasma, normal brain, and flank tumor in flank xenograft mice ($N = 4$-6). (C) Total drug concentration and (D) free drug concentration in plasma, intracranial tumor core (IC tumor core), and brain-around-tumor (BAT) in intracranial xenograft mice ($N = 3$-4). Dotted lines represent hypothetical effective concentrations, or IC_{50} values (1.08 μM based on total drug and 0.032 μM based on free drug). One-sample *t* tests were performed to compare the total and free concentrations with the respective total and free IC_{50} values at a significance level of 0.05 (* $P < 0.05$). The upward arrows and the listed values indicate the higher drug concentrations in the flank tumor versus normal brain in the flank xenograft mice, and those in the IC tumor core versus BAT in the intracranial xenograft mice. Data are presented as mean ± standard deviation (S.D.).

Figure 7. Total and free tissue-to-plasma ratios (single time point Kp and Kp,uu, respectively) at 1 and 6 hours after administration of a single oral dose (30 mg/kg) of ponatinib in GBM6 flank and intracranial xenograft mice for tumor distribution studies. (A) Kp in normal brain, flank tumor, and thigh muscle (non-cancerous) in flank xenograft mice ($N = 4$-6). (B) Kp,uu in normal brain and flank tumor in flank xenograft mice ($N = 4$-6). (C) Kp and (D) Kp,uu in the tumor core (IC tumor core) and brain-around-tumor (BAT) in intracranial xenograft mice ($N = 3$-4). One-sample *t* tests were performed to compare the experimental

JPET Fast Forward. Published on August 28, 2017 as DOI: 10.1124/jpet.117.243477
This article has not been copyedited and formatted. The final version may differ from this version.

values of tissue partition coefficients (Kp and Kp,uu) with the hypothetical value of 1 at a significance level of 0.05 (* $P < 0.05$). Dotted lines represent unity (Kp or Kp,uu at 1). The upward arrows and the listed DA values (DA_{total} or DA_{free}) indicate the higher tissue partition coefficients (Kp or Kp,uu) in the flank tumor versus normal brain in the flank xenograft mice, and those in the IC tumor core versus BAT in the intracranial xenograft mice. Data are presented as mean ± standard deviation (S.D.).

Figure 8. A hypothetical schematic of the equilibration of free (unbound) drug delivery between plasma (blood) and tumor sites (flank or orthotopic tumor). (A) The movement of free drugs in the absence of the blood-tissue barrier in PDX mice with flank xenograft and in the presence of the blood-brain barrier (BBB) in PDX mice with orthotopic xenograft. (B) Relative BBB integrity throughout the brain bearing GBM tumor. (C) Relatively restricted free drug delivery to the growing edge (brain-around-tumor, BAT) of orthotopic tumor and resultant GBM invasion throughout the rest of brain.

JPET Fast Forward. Published on August 28, 2017 as DOI: 10.1124/jpet.117.243477
This article has not been copyedited and formatted. The final version may differ from this version.

TABLES

Table 1. Pharmacokinetic/metric parameters determined by noncompartmental analysis of total and free drug concentrations in the brain and plasma, following serial sacrifice (destructive sampling) after a single oral dose (30 mg/kg) of ponatinib in FVB wild-type mice. Data are presented as mean or mean ± standard error of the mean (S.E.M.)

	Plasma		**Brain**	
	Free drug	**Total drug**	**Free drug**	**Total drug**
Half-life (hr)	-	4.4	-	5.7
Tmax (hr)	-	2	-	2
Cmax (μM) (Mean ± S.E.M)	0.0044 ± 0.00041	1.93 ± 0.18	0.00050 ± 0.000036	1.69 ± 0.12
$AUC_{(0-t)}$ (hr*μM) (Mean ± S.E.M.)	0.042 ± 0.0026	18.3 ± 1.13	0.0043 ± 0.00035	14.6 ± 1.21
$AUC_{(0-\infty)}$ (hr*μM)	0.043	18.9	0.0046	15.5
Vd/F (L/kg)	-	17.6	-	-
CL/F (mL/min/kg)	-	46.6	-	-
Kp ($AUC_{(0-\infty)}$ ratio)	-	-	-	0.82
Kp,uu ($AUC_{(0-\infty)}$ ratio)	-	-	0.11	-
Kp (transient steady-state)	-	-	-	0.87
Kp,uu (transient steady-state)	-	-	0.11	-

Tmax, time at the maximum drug concentration

Cmax, maximum drug concentration

$AUC_{(0-\infty)}$, area under the curve from zero to time infinity

Vd/F, apparent volume of distribution

CL/F, apparent clearance

JPET Fast Forward. Published on August 28, 2017 as DOI: 10.1124/jpet.117.243477
This article has not been copyedited and formatted. The final version may differ from this version.

Kp (AUC ratio), the ratio of $AUC_{(0-\infty,brain)}$ to $AUC_{(0-\infty,plasma)}$ using total drug concentrations

Kp,uu (AUC ratio), the ratio of $AUC_{(0-\infty,brain)}$ to $AUC_{(0-\infty,plasma)}$ using free drug concentrations

Kp (transient steady-state), the ratio of the maximum total brain concentration to the corresponding total plasma concentration at that time

Kp,uu (transient steady-state), the ratio of the maximum free brain concentration to the corresponding free plasma concentration at that time

JPET Fast Forward. Published on August 28, 2017 as DOI: 10.1124/jpet.117.243477
This article has not been copyedited and formatted. The final version may differ from this version.

Table 2. Free fraction (fu) values determined from in vitro rapid equilibrium dialysis (RED) experiment after 4-hour incubation in triplicate. Data are presented as mean ± standard deviation (S.D.).

Matrix	fu value (%) (Mean ± S.D.)
Serum-containing media	2.99 ± 0.089
Plasma	0.23 ± 0.068
Normal brain	0.029 ± 0.0085
Brain-around-tumor (BAT)	0.023 ± 0.0014
Intracranial tumor core	0.12 ± 0.051
Flank tumor	0.088 ± 0.024

fu, free (unbound) fraction of drug

JPET Fast Forward. Published on August 28, 2017 as DOI: 10.1124/jpet.117.243477
This article has not been copyedited and formatted. The final version may differ from this version.

FIGURES

Figure 1.

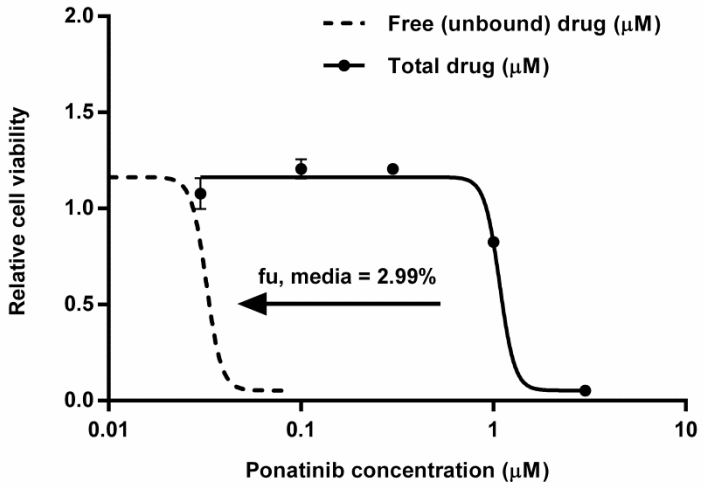

JPET Fast Forward. Published on August 28, 2017 as DOI: 10.1124/jpet.117.243477
This article has not been copyedited and formatted. The final version may differ from this version.

Figure 2.

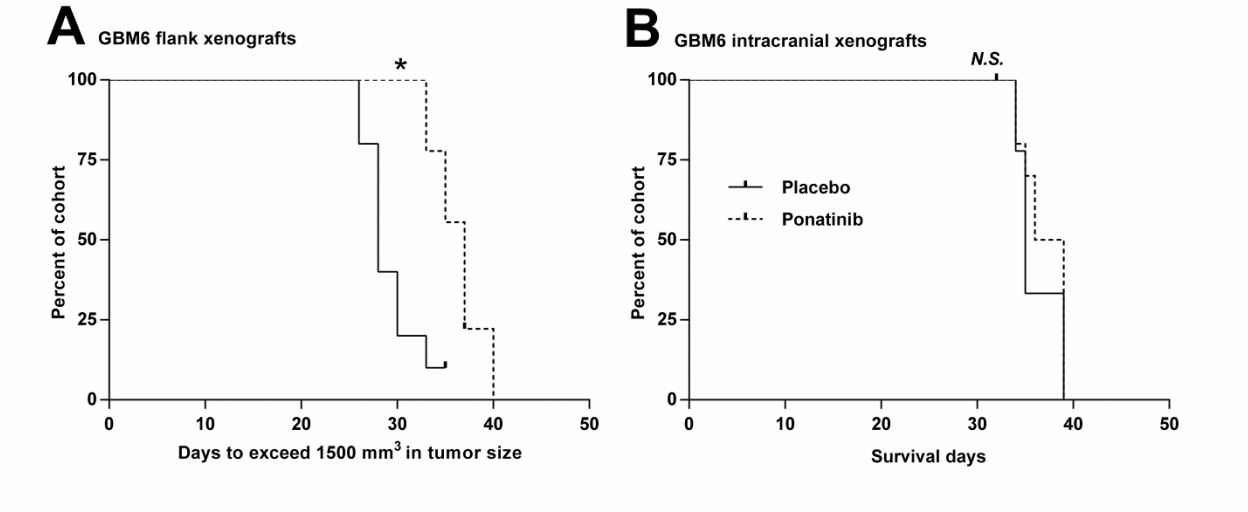

JPET Fast Forward. Published on August 28, 2017 as DOI: 10.1124/jpet.117.243477
This article has not been copyedited and formatted. The final version may differ from this version.

Figure 3.

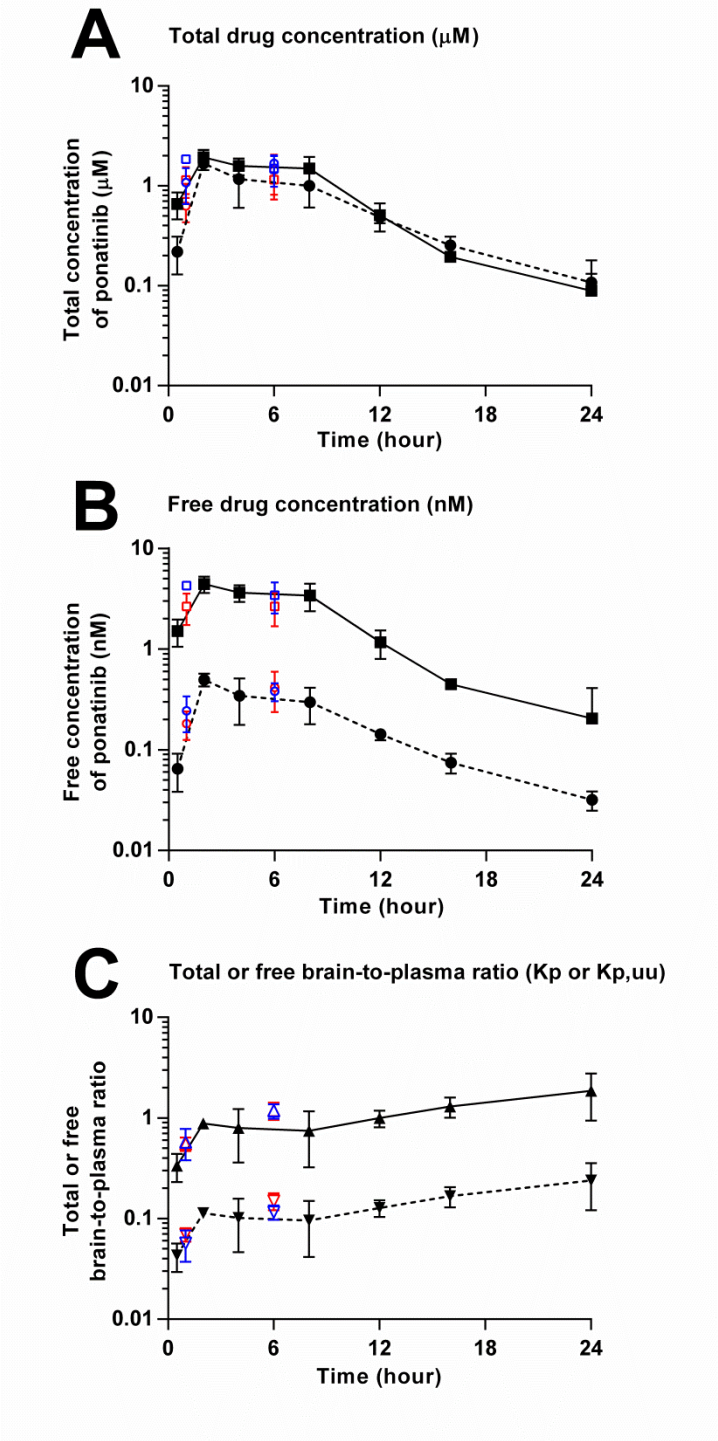

JPET Fast Forward. Published on August 28, 2017 as DOI: 10.1124/jpet.117.243477
This article has not been copyedited and formatted. The final version may differ from this version.

Figure 4.

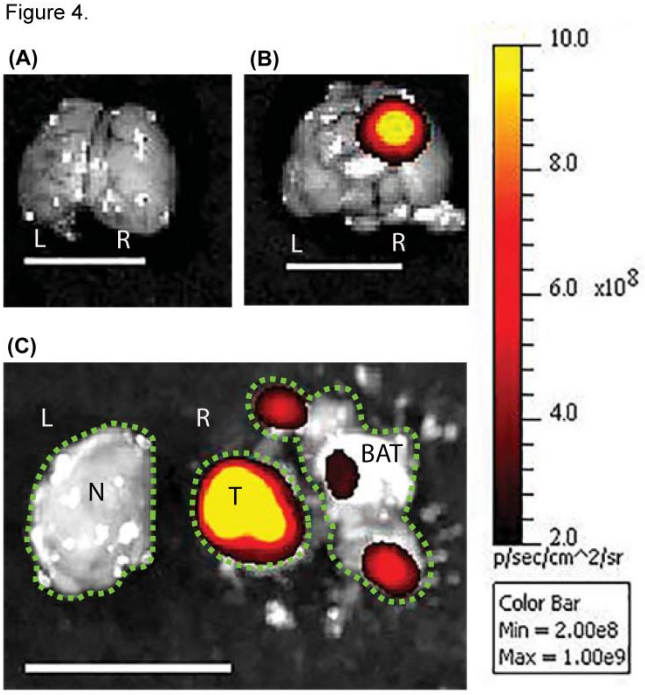

JPET Fast Forward. Published on August 28, 2017 as DOI: 10.1124/jpet.117.243477
This article has not been copyedited and formatted. The final version may differ from this version.

Figure 5.

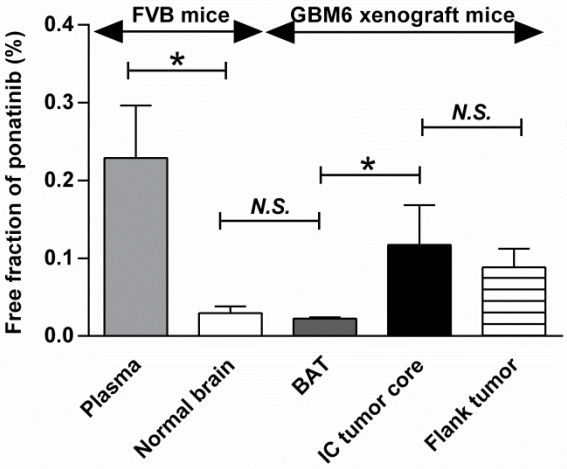

JPET Fast Forward. Published on August 28, 2017 as DOI: 10.1124/jpet.117.243477
This article has not been copyedited and formatted. The final version may differ from this version.

Figure 6.

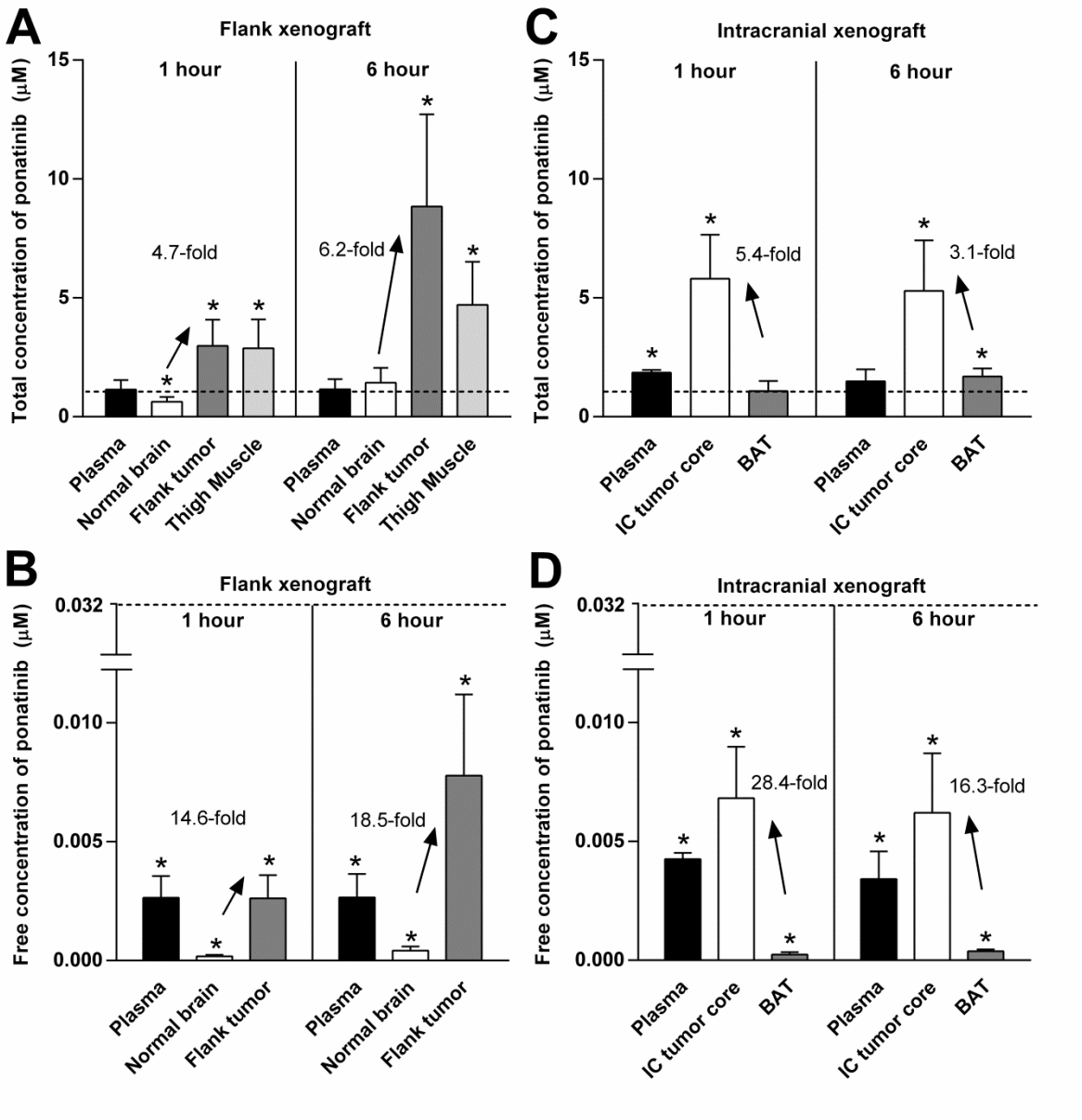

JPET Fast Forward. Published on August 28, 2017 as DOI: 10.1124/jpet.117.243477
This article has not been copyedited and formatted. The final version may differ from this version.

Figure 7.

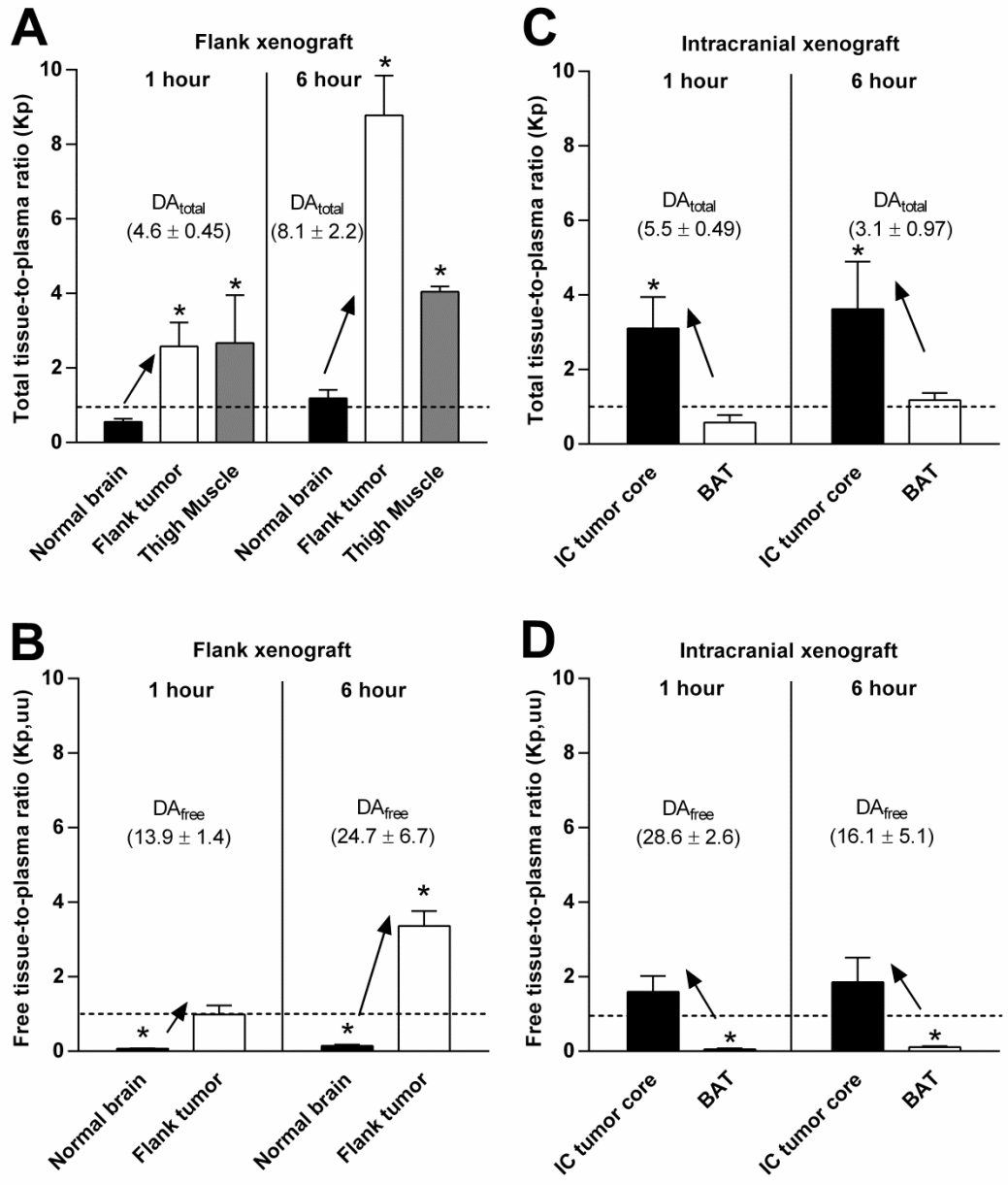

JPET Fast Forward. Published on August 28, 2017 as DOI: 10.1124/jpet.117.243477
This article has not been copyedited and formatted. The final version may differ from this version.

Figure 8.